

**FACULTY OF SCIENCE AND TECHNOLOGY
ADVANCED TECHNOLOGY
BACHELOR THESIS**

**ENHANCING SOFT-ROBOT MOBILITY:
INVESTIGATING SINGLE LEG MAGNETI-
ZATION FOR OMNIDIRECTIONAL MOTION**

JIM VAN DER VEEN

FACULTY OF ENGINEERING TECHNOLOGY
DEPARTMENT OF BIOMECHANICAL ENGINEERING

EXAMINATION COMMITTEE
PROF. DR. IR. S. MISRA
DR. V. KALPATHY VENKITESWARAN
DR. IR. M.P. DE JONG

JULY 10, 2024

UNIVERSITY OF TWENTE.

Thesis submitted by
Jim van der Veen
under the supervision of
Prof. dr. ir. S. Misra,
dr. V. Kalpathy Venkiteswaran, and
dr. ir. M.P. de Jong
in order to fulfill the necessary requirements to obtain a Bachelor's degree in
Advanced Technology at the University of Twente
and defended on
Wednesday, 10th of July, 2024

Abstract

Minimal Invasive Surgery (MIS) strives to improve patients' safety and reduce postoperative complications. Recent developments in soft robotics, in particular the field of magnetic actuation, have provided an outlook for untethered control and manipulation of these robots. Focus has shifted towards achieving omnidirectional motion, promising significant improvements in manoeuvrability, precise positioning, and usability in real-life scenarios. The study investigated the performance of three legs with different magnetization patterns on gait performance indicators using both a Cosserat rod model and an experiment. The gait performance was compared in a single-legged test where the results indicated competitive performance between straight and zigzag patterns, while the 90-degree magnetized leg showed inferior performance.

Table of Contents

Abstract	i
Table of Contents	ii
List of Figures	iii
List of Tables	iv
1 Introduction	1
2 Background	3
2.1 Magnetic actuation	3
2.2 Magnetic polymer composites	4
2.3 Cosserat rod	5
2.4 Gaits and effective gaits	7
2.4.1 Gaits	7
2.4.2 Performance indicators	8
3 Materials and Methods	11
3.1 Fabrication process	11
3.2 Magnetization properties	11
3.2.1 Straight leg	11
3.2.2 Zigzag	12
3.2.3 Rotation of 90°	13
3.3 Cosserat rod simulation	13
3.4 Experiments	13
3.4.1 Single-legged performance	13
3.5 Data processing	15
4 Results	16
4.1 Simulations	16
4.2 Maximum deflection	16
4.2.1 Deflection in the X direction	17
4.2.2 Deflection in the Y direction	18
4.2.3 Deflection in the Z direction	19
4.3 Power-/Return stroke ratio	20
4.4 Height Delta	21
5 Discussion	22
6 Conclusion and Future research	23
References	24
A Appendix	25
A.1 List of Parameters	25

List of Figures

1	The locomotion of the state-of-the-art omnidirectional robot.	1
2	An example millipede-inspired multi-legged soft robot [1].	2
3	An exemplary Helmholtz coil with a graph of the combined Magnetic Field Strength B/B_0 [2].	3
4	The composure of a MPC [3].	4
5	The magnetization process of a ferromagnetic material [4].	4
6	A schematical overview of the bending of an MPC due to magnetic actuation, with the red arrows indicating the dipole orientation inside of the legs [5].	5
7	A schematic of the four different deformations of the Cosserat rod [6].	6
8	The gait cycle of a human [7].	7
9	Views of the MPC leg suspended in a cast, with axes indicated.	8
10	A schematic view of T_p and T_r	9
11	The tested performance indicators displayed in the XZ-plane.	9
12	The tested performance indicators displayed in the XY-plane.	10
13	The fabrication process of an MPC leg [8].	11
14	The fabrication process of the Straight magnetized MPC. The moulds of the MPC are indicated in red, with the grey rectangles indicating the MPC legs.	12
15	The fabrication process of the Zigzag magnetized MPC. The moulds of the MPC are indicated in red, with the grey rectangles indicating the MPC legs.	12
16	The fabrication process of the 90-degree magnetized MPC. The moulds of the MPC are indicated in red, with the grey rectangles indicating the MPC legs.	13
17	A schematic of the setup for the Zigzag leg with dimensions indicated. (a) The width of the MPC leg, (b) the length of the MPC leg, (c) the height of the cast where the MPC leg is suspended within, (d) the width of the cast where the MPC leg is suspended within, (e) is the breadth of the cast where the MPC leg is suspended within, (f) is the breadth of the leg. \mathbf{B} indicates the direction of rotation of the magnetic field.	14
18	A top view of the setup, with arrows indicating the different magnetic field rotating directions. Angle 0° corresponds with a rotating field around $(0,1,0)$, angle 45° corresponds with a rotating field around $(1,1,0)$, angle 90° corresponds with a rotating field around $(1,0,0)$ and the 135° corresponds with a rotating field around $(-1,1,0)$	14
19	Extrema points with the red crosses indicating the measurement points at the tip position.	15
20	The results of the deflection of the simulated single legs at an angle of 0° under different magnetic fields.	16
21	The results of the single-legged performance of the three legs: The maximum deflection of the leg in the X direction.	17
22	The results of the single-legged performance of the three legs: The maximum deflection of the leg in the Y direction.	18
23	The results of the single-legged performance of the three legs: The maximum deflection of the leg in the Z direction.	19
24	The results of the single-legged performance of the three legs: The Power-/ Return Stroke ratio T_p/T_r	20
25	The results of the single-legged performance of the three legs: The height delta.	21
A.1	Dimensions of the Straight MPC mould.	26
A.2	Dimensions of the Zigzag MPC mould.	26
A.3	Dimensions of the 90-degree MPC mould.	27

List of Tables

1	Dimensions of the setup	15
A.1	Range of tested parameters for single-legged performance	25
A.2	Simulation parameters	25
A.3	Dimensions of the moulds	25

1 Introduction

The soft robotics field has experienced significant development over the years with a particular focus in the direction of soft robots capable of versatile motion. Versatile motion is especially useful in navigating complex and dynamic environments. In contrast to rigid robotics, soft robots, which are inspired by nature, offer unique capabilities such as flexibility, compliance, and dexterity, making them useful in a wide range of applications. A useful application for soft robots can be found in surgical environments. In the surgical context, soft robots could be used for so-called Minimally Invasive Surgery (MIS) [9]. During MIS, flexible soft robots could be inserted into small incisions. After being inserted into the patient, the robot could access the target anatomy directly and operate internally, minimizing the damage to the peripheral tissue. For these kinds of surgical applications, magnetically actuated soft robots offer a unique value proposition due to their ability to be controlled in a tetherless manner. This tetherless control is achieved by introducing magnetic particles into a silicone solution, forming a magnetic polymer composite (MPC). The MPC retains the mechanical flexibility of a regular silicone leg while exhibiting the magnetic properties of a permanent magnet, enabling magnetic actuation.

Research on soft robotics which is of particular interest is done in tandem actuation of legged locomotion [1] [10]. Fig. 2 shows an existing prototype made by the Surgical Robotics research group. This work introduces untethered magnetic soft robots with grasping manipulators capable of executing pick-and-place tasks. By leveraging external magnetic fields, they have achieved stable locomotion and efficient grasping, proving the potential for soft robots. However, despite the promising potential for soft robotics with legged locomotion, achieving the omnidirectional motion of such robots still poses a challenge. Omnidirectional motion refers to the capability of an object, or robot in our case, to move in any direction without changing orientation. The development of an omnidirectional soft robot would greatly improve manoeuvrability due to its ability to navigate tight spaces and its inherent ability for precise positioning, thus increasing usability in real-life scenarios.

State-of-the-art research in omnidirectional movement for soft robots was performed where researchers took a starfish as an example, embracing the example of biomimicry [11]. As a further proof of concept, a bachelor thesis on the omnidirectional movement of soft robotics was done by a student (with a nearly identical name to mine) at the University of Twente [8], result of which can be seen in Fig. 1. In this research, the proof of concept for an omnidirectional soft robot was made by building on the previously researched leg-like structure which creates a moment when actuated by a magnetic field.

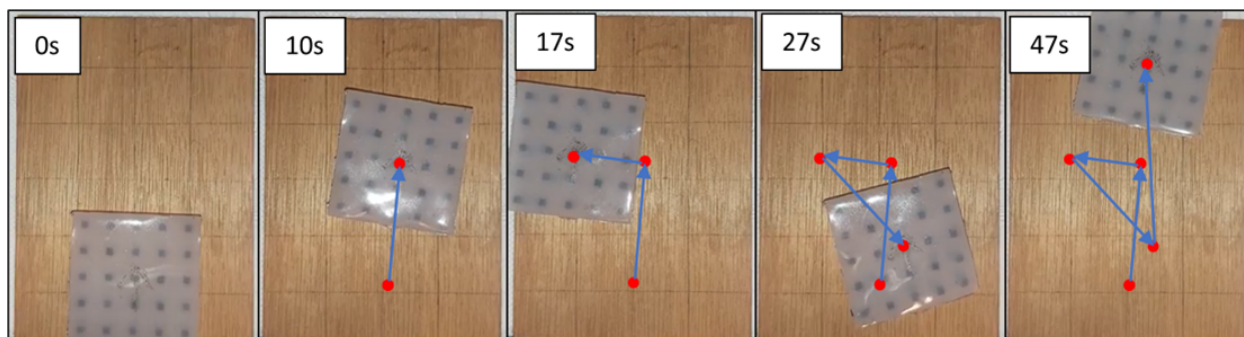


Figure 1: The locomotion of the state-of-the-art omnidirectional robot.

The proposed research aims to systematically explore how different magnetization patterns of legs affect performance indicators which are essential for the omnidirectional motion efficiency of soft robots. By varying the orientation, magnitude, and distribution of magnetic fields acting on the legs, this research seeks to explore their impact on locomotion efficiency, agility, and stability. This research utilizes the previous proof of concept as a foundation for its optimization. The relevance of this research lies in addressing the fundamental issues associated with achieving omnidirectional movement in soft robotics. By overcoming these challenges, this research aims to advance the research into soft robotics and unlock new opportunities in the application of soft robotics in various contexts.

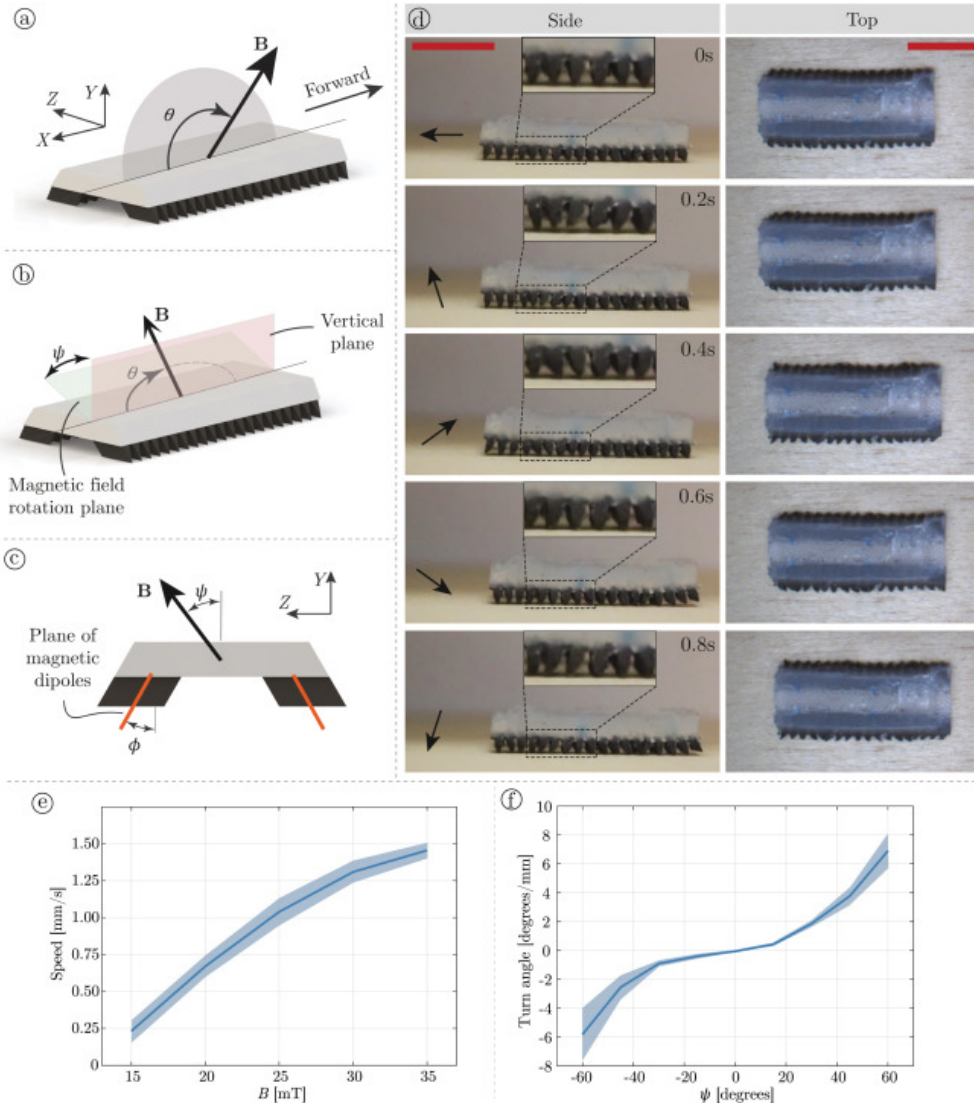


Figure 2: An example millipede-inspired multi-legged soft robot [1].

2 Background

In this section, a theoretical background for experimentation and modelling will be provided.

2.1 Magnetic actuation

One way to achieve untethered control of a soft robot is by exposing a (ferro)magnetic material to an external magnetic field to excite a force and torque acting on the material. In this research, a near-homogenous magnetic field \mathbf{B} was applied by a three-axis Helmholtz coil pair. Figure 3 illustrates an example of the magnetic field by a Helmholtz coil pair.

Given this setup, the force \mathbf{F}_m and torque $\boldsymbol{\tau}_m$ acting upon the magnetic material can be described using Eqns. (1)-(2)

$$\mathbf{F}_m = \int_V (\mathbf{M} \cdot \nabla \mathbf{B}) dV \quad (1)$$

$$\boldsymbol{\tau}_m = \int_V (\mathbf{M} \times \mathbf{B}) dV \quad (2)$$

In Eqns. (1)-(2) \mathbf{M} represents the internal magnetization per unit volume of the material, \mathbf{B} describes the external magnetic field acting upon this material and this dot- or cross product is then taken over the volume integral of the volume of this infinitesimally small volume.

In our case, the experiments were conducted in a three-axis Helmholtz coil pair, and the volume of the our magnet is relatively small. Therefore the field can assumed to be homogenous which gives $\nabla \mathbf{B} = 0$ and B can be considered to be constant. Given this, Eqns. (1)-(2) simplify to Eqns. (3)-(4) respectively.

$$\mathbf{F}_m = \boldsymbol{\mu} \cdot \nabla \mathbf{B} = 0 \quad (3)$$

$$\boldsymbol{\tau}_m = \boldsymbol{\mu} \times \mathbf{B} \quad (4)$$

Here, $\boldsymbol{\mu}$ represents the magnetic moment of the permanent magnet. Eqn. (3) shows that the magnetic force \mathbf{F}_m is zero in a homogeneous magnetic field as $\nabla \mathbf{B} = 0$. Eqn. (4) indicates that the magnetic torque $\boldsymbol{\tau}_m$ is determined by the cross product of the magnetic moment and the magnetic field of the Helmholtz coil setup. Eqn. (4) serves as the working principle for the untethered movement of the soft robots under magnetic actuation.

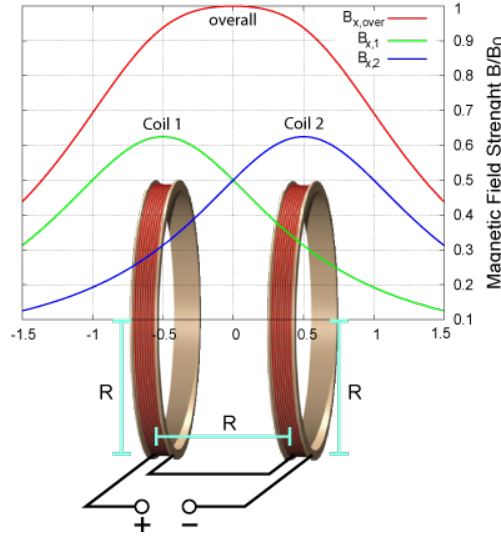


Figure 3: An exemplary Helmholtz coil with a graph of the combined Magnetic Field Strength B/B_0 [2].

2.2 Magnetic polymer composites

Magnetic polymer composites (MPCs) are materials which combine the properties of polymers with magnetic particles. These composites leverage the advantages of the flexibility of the polymers with the responsiveness to magnetic actuation of the ferromagnetic particles mixed within. This results in a soft material which can be actuated and controlled through external magnetic fields. Fig. 4 shows the composure of a MPC material.

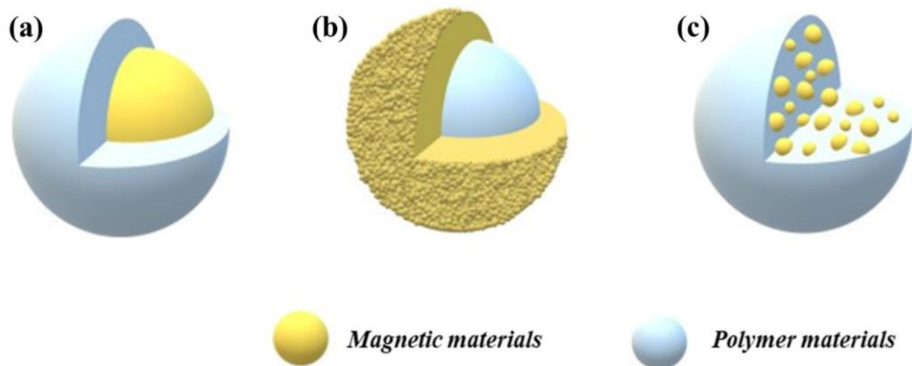


Figure 4: The composure of a MPC [3].

The main advantages lie not only within the flexibility and magnetic responsiveness, but also in the customizability of such materials. By varying the type, concentration of the magnetic particles, as well as the polymer, the mechanical and magnetic properties of MPCs can be finely tuned in order to meet specific application requirements.

The magnetic particles embedded in this polymer however still need to undergo a crucial step post-fabrication such that the magnetic dipole domains within the magnetic particles are properly aligned. This process consists of exposing the MPC to a strong external magnetic field, whereafter the magnetic dipoles orient themselves in a uniform magnetization pattern. Fig. 5 the magnetization process is illustrated.

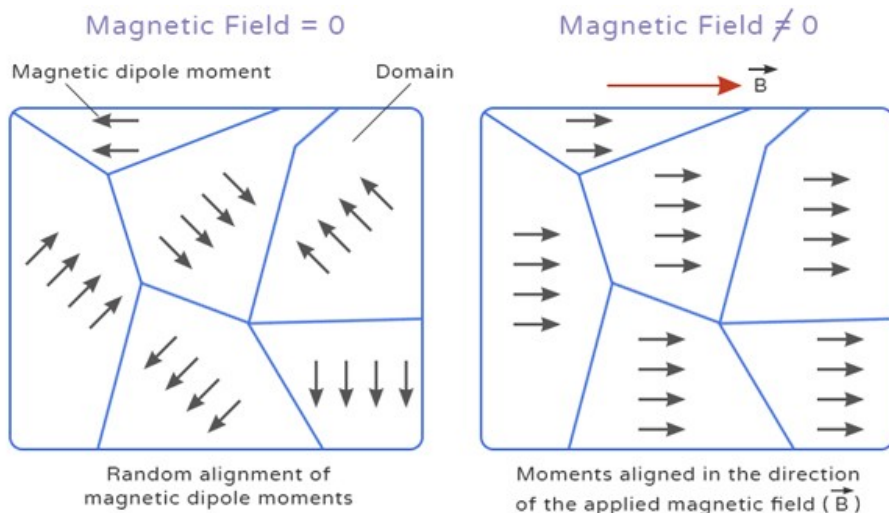


Figure 5: The magnetization process of a ferromagnetic material [4].

By orienting these magnetic dipoles in a uniform magnetization pattern, it enables the composite to respond effectively to external magnetic actuation. In this research, we are particularly interested in different

magnetization patterns of MPC legs. Therefore, we will further define the magnetization pattern $\phi(s)$ (how these dipoles are oriented inside of the MPC) and magnetization per unit volume μ_V (how strongly magnetized the MPC is) along the legs. This is described by Eqn. (5)

$$\mu(s) = R_y(\theta(s)) \cdot R_y(\phi(s)) \cdot [\mu_V V_A; 0] \quad (5)$$

In this equation, R_y is a rotation matrix around the z-axis and $\mu(s)$ is the dipole per unit length. The variable s represents the distance along the leg, $\theta(s)$ represents the angle between the x-axis and the leg segment and $\phi(s)$ is the magnetization pattern angle of the leg and $\mu_V = \frac{1}{\mu_0} B_r$ is the magnetization per unit volume. V_A is the volume of the segment of the leg. These parameters are also displayed as a schematic drawing in Fig. 6. The angle $\phi(s)$ will be defined for the different legs in the materials section. The angle ϕ allows us to model how the magnetization pattern changes along the leg, which is crucial for simulating the legs.

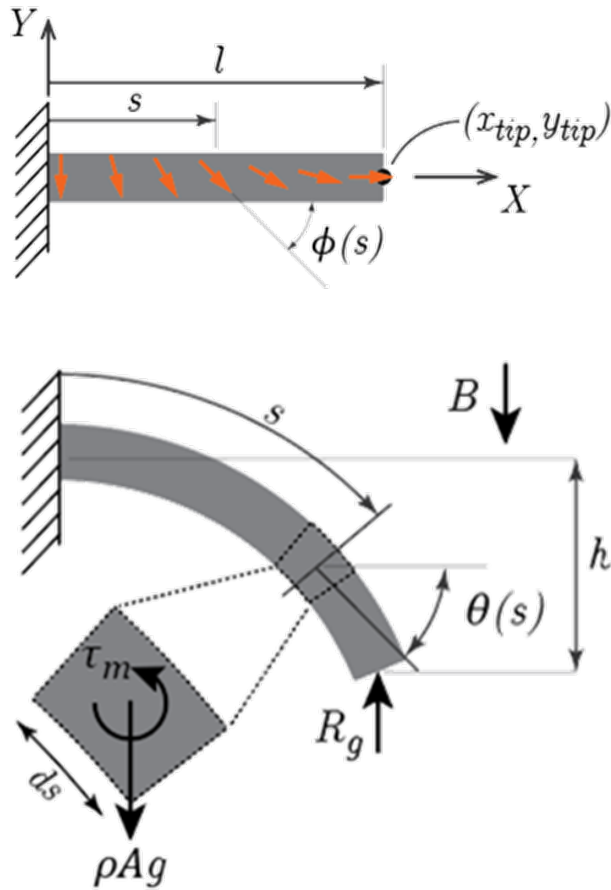


Figure 6: A schematical overview of the bending of an MPC due to magnetic actuation, with the red arrows indicating the dipole orientation inside of the legs [5].

2.3 Cosserat rod

The simulation of the single-legged performance for the different legs is based on the Cosserat rod model, which is favoured above the classical beam theories like Euler-Bernoulli or Timoshenko beam theories for one reason. During the movement of the MPC legs under magnetic actuation, shear and torsion effects occur. Traditional beam theories do not take this into account, therefore the Cosserat rod model is considered to be geometrically exact and chosen as the theory of choice.

In the Cosserat model, the deformations of the leg are divided in four types, defined such as in Fig. 7. In the implemented MATLAB code, inspired by another bachelor student at the SRL research group, these four categories are all represented [12]. The bending and torsional deformations are, however, dominant during the magnetic actuation of MPC. We are therefore more interested in the curvature strain vector \mathbf{u} of the Cosserat rod as in Eqn. (6)

$$\mathbf{u} = \begin{bmatrix} u_1 \\ u_2 \\ u_3 \end{bmatrix} \quad (6)$$

- u_1 and u_2 : Indicate the amount of bending per unit length [rad/m] in the directions of the principal axes of the cross-section. If u_1 is non-zero, the rod is bending in the plane defined by the x_2 and x_3 axes. Similarly, a non-zero u_2 indicates bending in the plane defined by the x_1 and x_3 axes
- u_3 : Indicates the rate of twist per unit length [rad/m] about the longitudinal axis of the rod. A non-zero u_3 implies that the rod is experiencing torsion.

The curvature strain vector \mathbf{u} is further defined such as in Eqn. (7):

$$\mathbf{u} = \mathbf{K}_{bt} (\mathbf{R}'m) + \mathbf{u}^* \quad (7)$$

where \mathbf{K}_{bt} is the stiffness matrix of the material, $\mathbf{R}'m$ is a rotation matrix to match the coordinate systems of the stiffness matrix to the coordinate system of the segment and \mathbf{u}^* incorporates any additional displacement effects that are not directly related to the bending and torsional response captured by \mathbf{K}_{bt} . These formulas form the basis for the BVP which is the Cosserat rod model. This is incorporated in a MATLAB code and simulated for the theoretical single-legged performance characteristics.

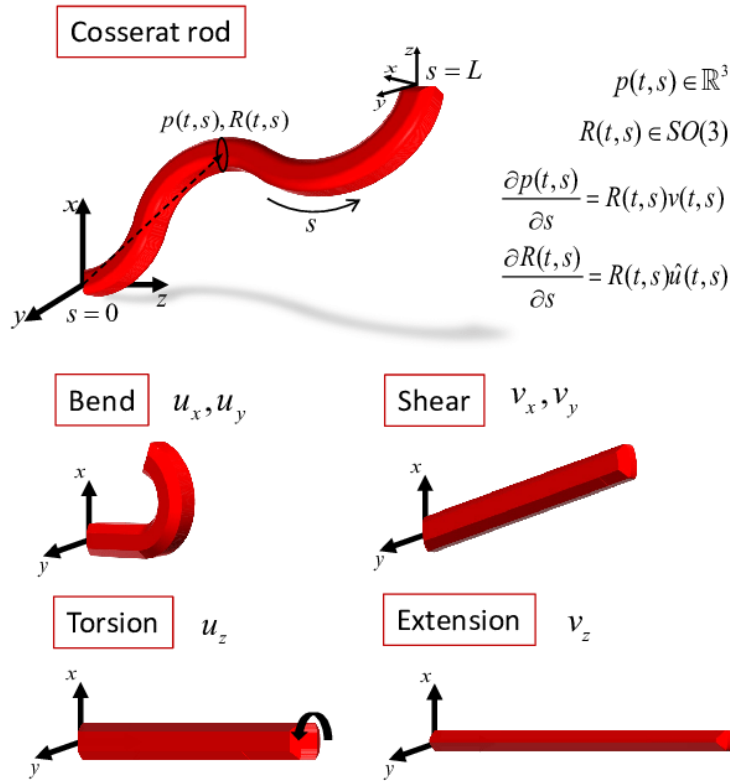


Figure 7: A schematic of the four different deformations of the Cosserat rod [6].

2.4 Gaits and effective gaits

Locomotion is described as the act of something moving or transporting itself from one place to another. Different types of locomotion are for example: walking, running, crawling, rolling, flying, climbing, swimming, skipping and jumping. For a primary example, we can observe the walking of a person, as illustrated in Fig. 8.

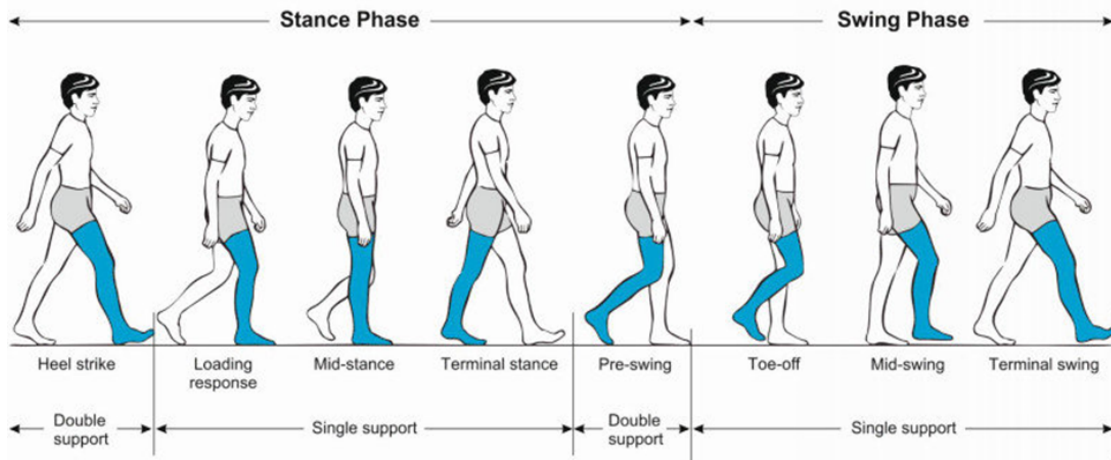


Figure 8: The gait cycle of a human [7].

A person goes through a so-called gait cycle. Gait refers to a person’s manner of locomotion. In this cycle, several parameters can be defined which will serve as performance indicators for the efficiency of the walk. This section serves to give a background on gaits and how biomimicry can inspire soft robot design.

2.4.1 Gaits

In this subsection, we will showcase two examples of gaits from human leg and hexapods. Different animals have different kind of gaits. We will discuss two kinds of animal gaits and their potential relevance for our research case.

Human Gait Cycle

Humans have a gait cycle as seen in Fig. 8. The human gait cycle starts at a double support of both legs. The cycle can be broken down into two main phases/strokes:

1. **Stance Phase:** This starts with a heel strike, whereafter all the weight of the body gets supported by this leg. The leg then supports the body while the other leg wings forward.
2. **Swing Phase:** The leg that was supporting the body now swings forward to prepare again for the next heel strike. This swing phase then restarts at the stance phase and so the cycle continues.

For our research purposes, we are interested in the single-legged characteristics of this gait cycle, particularly the transition from the stance phase to the swing phase, which we will now refer to as the power stroke and the return stroke.

Hexapod Gait Cycle

Hexapods, such as arachnids or insects, exhibit an approach which is very different. Their gait cycle typically involves a coordinated movement of multiple legs. This mostly happens with using a tripod gait, where three legs are always in contact with the ground while the other three legs swing forward. This movement provides stability and continuous support for the body making it efficient and adaptable to a wide range of terrains.

2.4.2 Performance indicators

To determine how well suited the selected gait is for omnidirectional motion, gaits can be given certain performance indicators. In this section, three performance indicators will be explained which provide the basis of the experiments conducted. Figs. 9a-9b show the axes systems of a MPC leg in a cast to help visualize the performance indicators better.

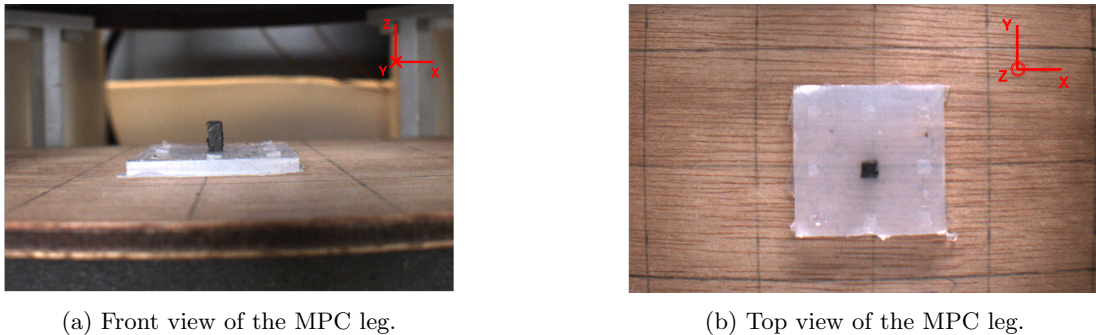


Figure 9: Views of the MPC leg suspended in a cast, with axes indicated.

1. Maximum deflection:

The maximum deflection of the leg indicates the responsiveness of the MPC under an external magnetic field \mathbf{B} . This deflection is measured in all three axes. Deflection in the direction of movement (compliant direction) is favourable, deflection in the non-compliant direction (not aligned with the desired path) would not be wanted as this would mean a deviation from the intended trajectory. Hence, the maximum deflection provides an indication of the magnetic actuation efficiency and is crucial for achieving effective omnidirectional movement.

2. Power-/Return stroke ratio:

The gait cycle is divided into a power stroke and a return stroke. During the power stroke, the leg exerts force on the ground, facilitating a partial liftoff of the supporting body. After this power stroke, the leg returns to the starting position where it is able to exert power unto the ground again, therefore it returns to this position during the return stroke. We hypothesise that for optimal efficient locomotion, the ratio between the duration of the power stroke (T_p) to the return stroke (T_r) should be maximized. This ratio, denoted as T_p/T_r , is important for omnidirectional motion because a higher ratio means more time is spent applying force in the desired direction of movement, thereby enhancing propulsion and stability in all directions. This efficiency in the gait cycle directly contributes to smoother and more controlled omnidirectional locomotion.

3. Height Delta:

The height delta is the difference in height between the power stroke and the return stroke. This height delta is indicative of the distance the leg can lift the supporting body off the ground, which aids movement speed. A zero height delta would indicate that the leg would be rocking forwards and backwards without displacing the body. A larger height delta suggests more efficient locomotion, as it indicates a greater ability to lift and propel the body forward with each stroke, thereby enhancing overall movement efficiency and speed.

These performance indicators are schematically shown Figs. 10-12.

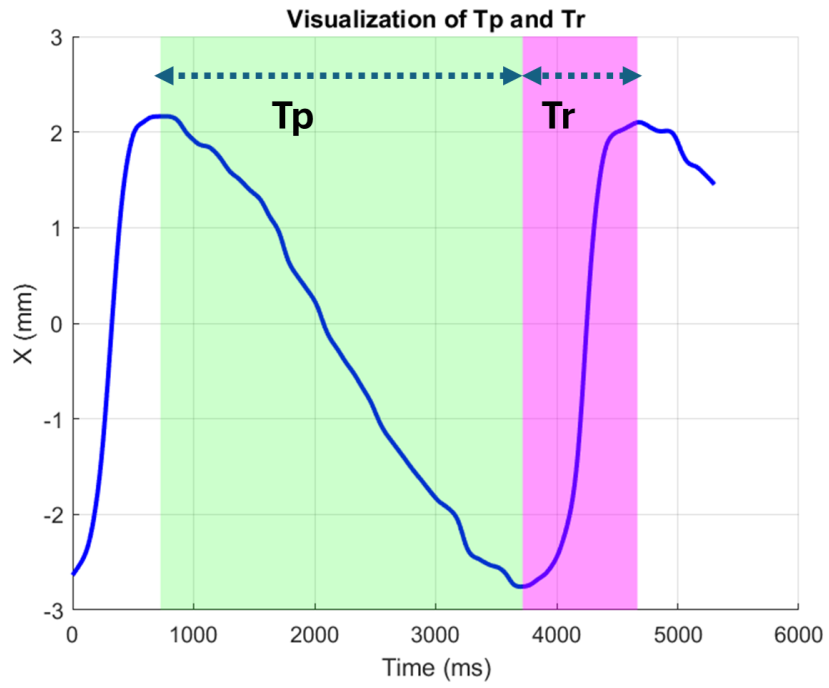


Figure 10: A schematic view of T_p and T_r .

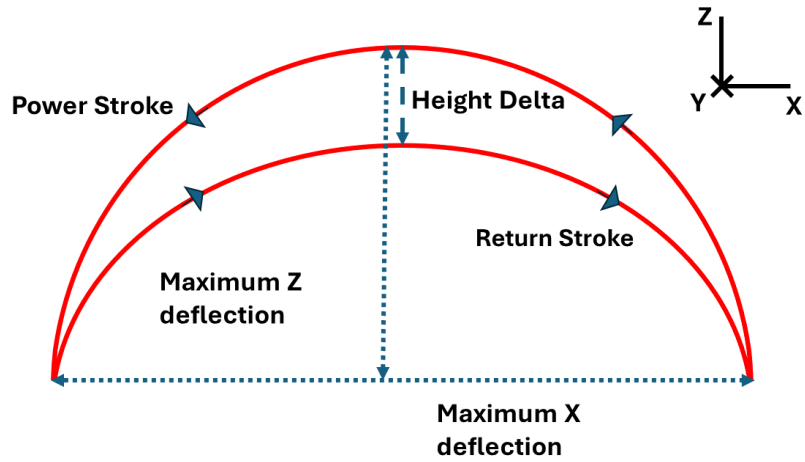


Figure 11: The tested performance indicators displayed in the XZ-plane.

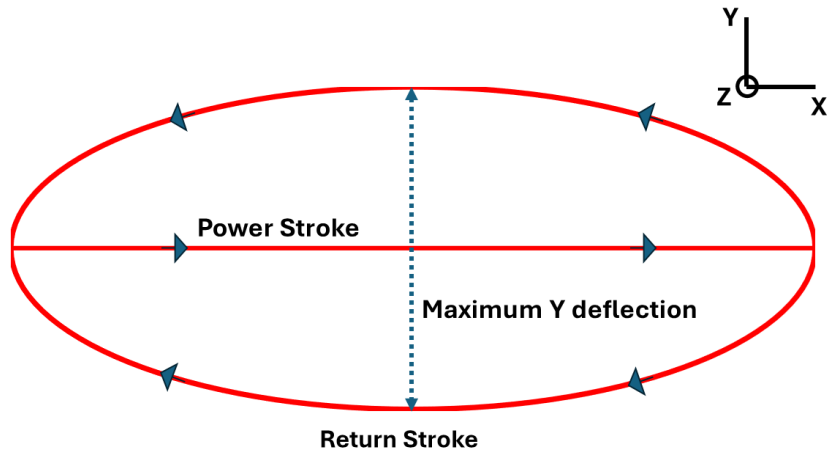


Figure 12: The tested performance indicators displayed in the XY-plane.

The methodology for testing these parameters for all leg magnetization configurations is further elaborated on in the experiments and data analysis sections 3.4.

3 Materials and Methods

In this section, the materials, fabrication process and methodology are expanded upon. It aims to provide insight into the steps to create a setup to test the previously described performance indicators.

3.1 Fabrication process

To create the final design the legs were first produced by mixing ferromagnetic powder (PrFeB) with a mean particle size of $5\mu m$ with silicon rubber to form a magnetic polymer composite (MPC). The silicon rubber (Ecoflex 00-20, Smooth-On, Inc., USA) is formed by mixing two liquid parts in a 1:1 mass/weight ratio, and then thoroughly mixed [13]. The magnetic powder is then also mixed with a ratio of 1:1 to the combined liquids. This mixture was then put in a vacuum chamber to remove air pockets from the mixture. This mixture was then cast into a mould composed of multiple acrylic plates and left to cure for 24 hours, forming the MPC legs. A schematic of this process can also be seen in Fig. 13.

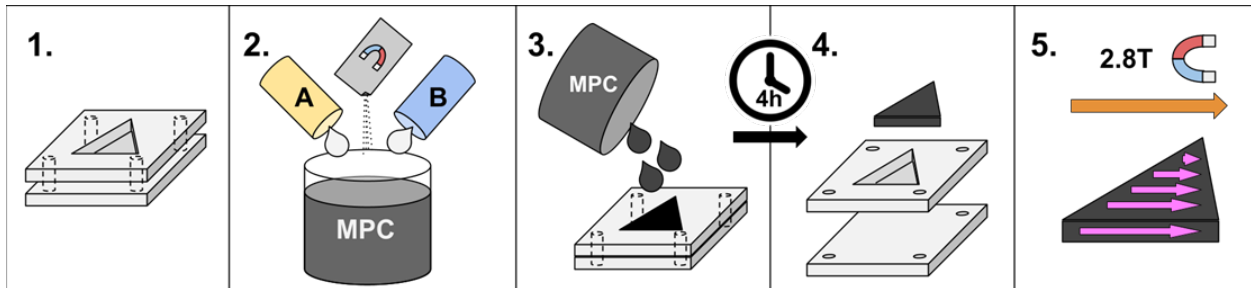


Figure 13: The fabrication process of an MPC leg [8].

3.2 Magnetization properties

To get the required magnetic actuation response of the MPC legs, the legs were put into a shaped mould to ensure the required magnetic dipole orientation was achieved. The MPC legs were then magnetized with a strong external magnetic field such that the dipoles would orient themselves towards the required direction.

3.2.1 Straight leg

The straight leg design is inspired by the state of the art and aims to serve as a benchmark for the other designs. For the straight leg, a simple mould was used. This mould was put axially in the magnetizer to get the required magnetization pattern. The corresponding magnetization pattern angle of the leg is given in Eqn. (8).

$$\phi(s) = 0 \tag{8}$$

This magnetization pattern angle and fabrication process is displayed in Fig. 14.

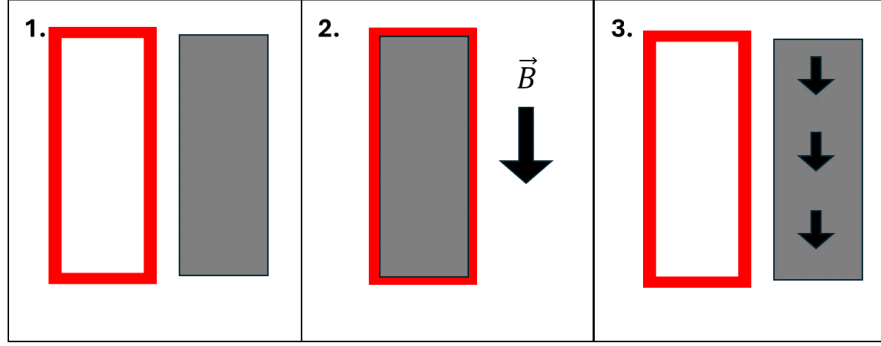


Figure 14: The fabrication process of the Straight magnetized MPC. The moulds of the MPC are indicated in red, with the grey rectangles indicating the MPC legs.

3.2.2 Zigzag

The Zigzag design is inspired by the human locomotion patterns and consists of a series of vertical zigzag bends. The corresponding magnetization pattern angle of the leg is given in Eqn. (9).

$$\phi(s) = \begin{cases} -\frac{\pi}{6} & \text{for } 0 \leq s < \frac{l}{3} \\ \frac{\pi}{6} & \text{for } \frac{l}{3} \leq s < \frac{2l}{3} \\ -\frac{\pi}{6} & \text{for } \frac{2l}{3} \leq s \leq l \end{cases} \quad (9)$$

The manufacturing process of the Zigzag leg is displayed in Fig.15.

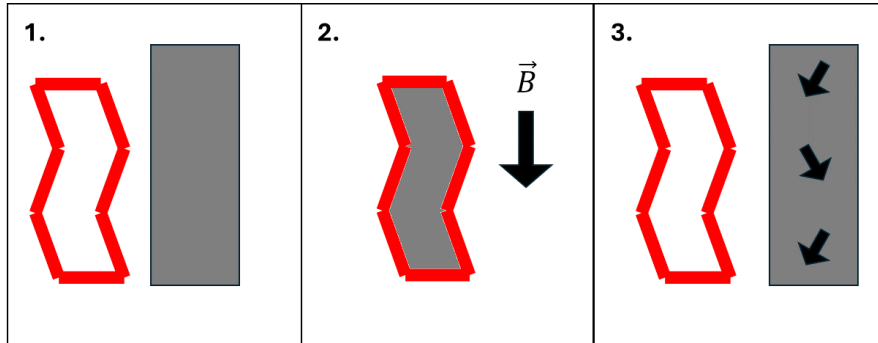


Figure 15: The fabrication process of the Zigzag magnetized MPC. The moulds of the MPC are indicated in red, with the grey rectangles indicating the MPC legs.

3.2.3 Rotation of 90°

This leg's magnetization pattern angle is largely hexapod inspired with its magnetization following a rotation of 90° over the length of the leg. The corresponding magnetization pattern angle is shown in Eqn. (10).

$$\phi(s) = \frac{\pi s}{2l} \quad (10)$$

The manufacturing process of the 90-degree leg is displayed in Fig.16.

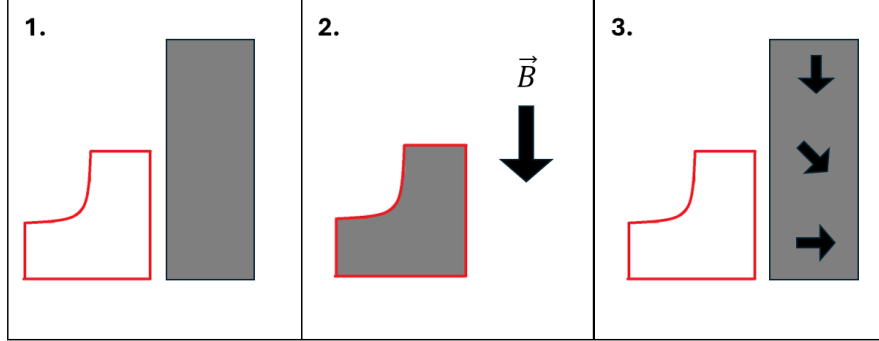


Figure 16: The fabrication process of the 90-degree magnetized MPC. The moulds of the MPC are indicated in red, with the grey rectangles indicating the MPC legs.

The dimensions of the different moulds and legs can be found in the appendix in Figs. A.1-A.3 and Table A.3.

3.3 Cosserat rod simulation

To verify the accuracy of the simulation, experiments were run under comparable conditions. All the parameters such as found in A.2 are chosen to match those of the fabricated MPC as closely as possible and are based on data found in specification sheets [13] and previous theses [8]. The Cosserat rod simulation was then tested on the maximum deflection and compared to the results of the physical experiments.

3.4 Experiments

3.4.1 Single-legged performance

In this experiment, three legs with different magnetization patterns were positioned in the centre of the Helmholtz coils. The three different legs were exposed to a rotating magnetic field as seen in Fig 18. The experiment was recorded using two FLIR Blackfly[©] S USB3 cameras, capturing the front and top views of the MPC legs. The footage was captured at 30 FPS using the program FLIR SpinView[©] software for optimal analysis. The movement of the leg was recorded for two full cycle times of the rotating magnetic field \mathbf{B} to ensure accuracy in the data processing. The testing angle of the legs is based on a rotation around the Z-axis from 0° to 135° with 0° being the angle as the legs were magnetized as seen in the fabrication section. The setup can be seen in Fig. 17. A schematic of these angles is shown in Fig. 18.

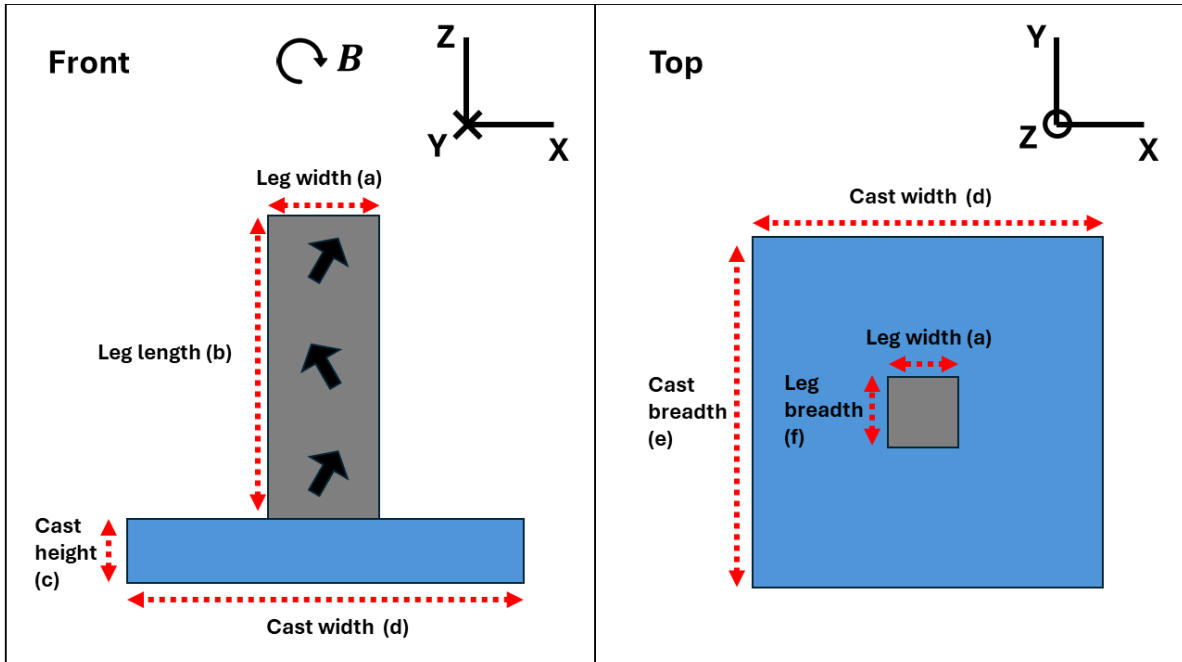


Figure 17: A schematic of the setup for the Zigzag leg with dimensions indicated. (a) The width of the MPC leg, (b) the length of the MPC leg, (c) the height of the cast where the MPC leg is suspended within, (d) the width of the cast where the MPC leg is suspended within, (e) is the breadth of the cast where the MPC leg is suspended within, (f) is the breadth of the leg. B indicates the direction of rotation of the magnetic field.

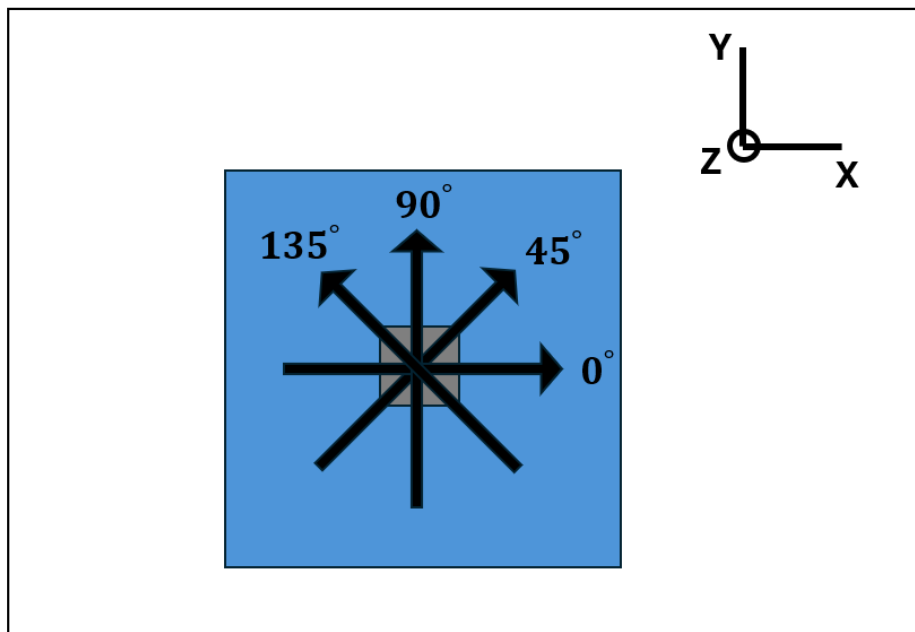
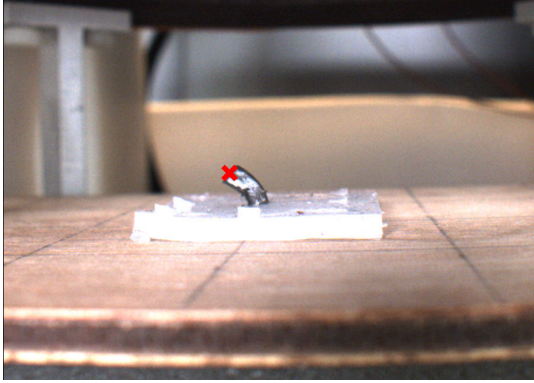
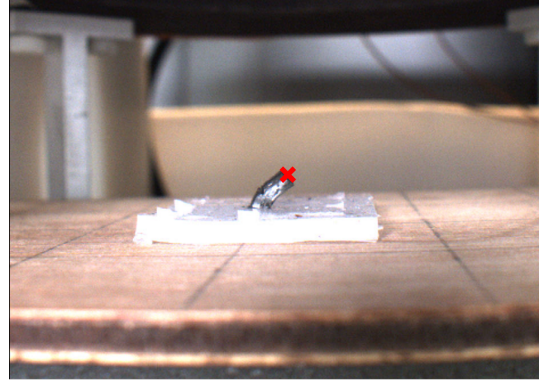


Figure 18: A top view of the setup, with arrows indicating the different magnetic field rotating directions. Angle 0° corresponds with a rotating field around $(0,1,0)$, angle 45° corresponds with a rotating field around $(1,1,0)$, angle 90° corresponds with a rotating field around $(1,0,0)$ and the 135° corresponds with a rotating field around $(-1,1,0)$.



(a) Leftmost point of the MPC leg.



(b) Rightmost point of the MPC leg.

Figure 19: Extrema points with the red crosses indicating the measurement points at the tip position.

For measurement accuracy, the sample was chosen to be rotated instead of choosing for a change in the rotation angle of the magnetic field. This ensured that the cameras would have a similar view with all tested angles, improving accuracy in data processing. Detailed testing parameters can be found in the appendix in table A.1. The setup can be seen in Fig. 17.

Table 1: Dimensions of the setup

Indicator	Description	Value	Unit
a	Leg width	2	mm
b	Leg length	5	mm
c	Cast height	1	mm
d	Cast width	25	mm
e	Cast breadth	25	mm
f	Leg breadth	2	mm

3.5 Data processing

The recorded videos of the magnetic actuation of the legs were processed in Kinovea, a video player tracker for sports analysis. In this program, one can track the trajectory of a point in a video over time, allowing for the three-dimensional tracking of an object over time. From the side camera, the vertical and horizontal positions can then be combined to make a spread plot of the tip positions in the compliant direction. Next to that, the top camera can be used to get the movement in the non-compliant direction. From this data, the three performance indicators can be determined.

4 Results

This section presents the results of the simulation and experiment data for the single-legged samples. The results are divided into the results from the different performance indicators: maximum deflection in the X, Y and Z directions, T_p/T_r and the height delta.

4.1 Simulations

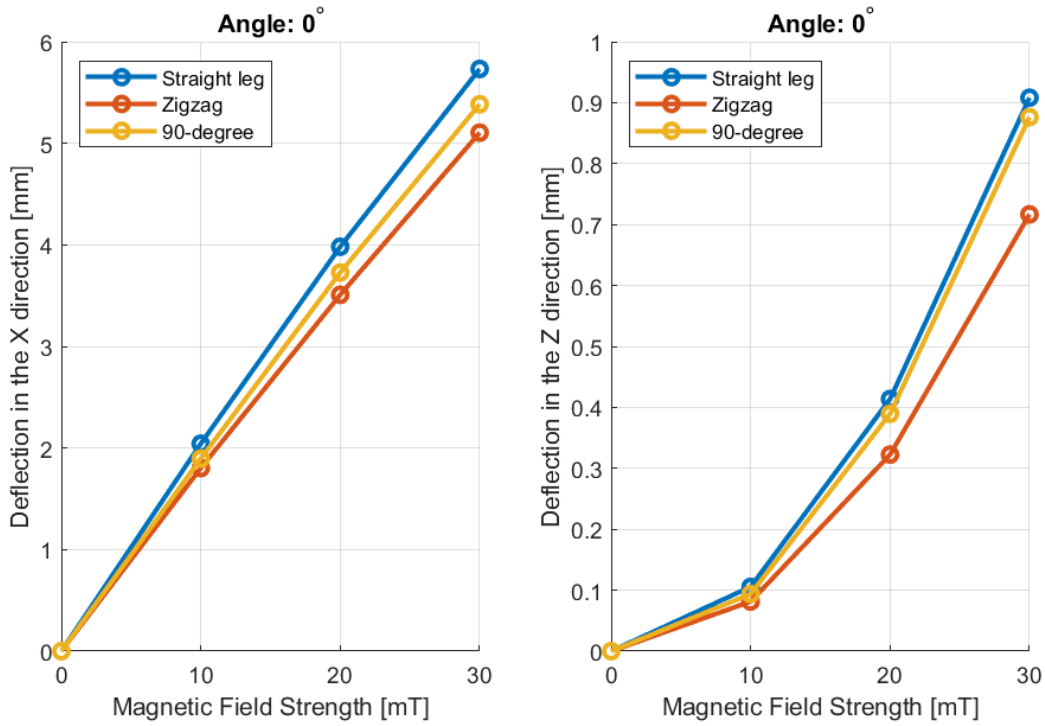


Figure 20: The results of the deflection of the simulated single legs at an angle of 0° under different magnetic fields.

In Fig. 20, the results for the deflection in the X direction and Z direction under various magnetic fields are displayed. From these results, it can be observed that the straight leg yields the highest deflection in the X and Z directions with the 90-degree leg and Zigzag leg following closely behind.

4.2 Maximum deflection

In this section the results of the deflection of the leg in each axis for the different directions are shown. The directions $[0^\circ, 45^\circ, 90^\circ, 135^\circ]$ correspond with the angles given in table A.1 and displayed schematically in Fig. 18.

4.2.1 Deflection in the X direction

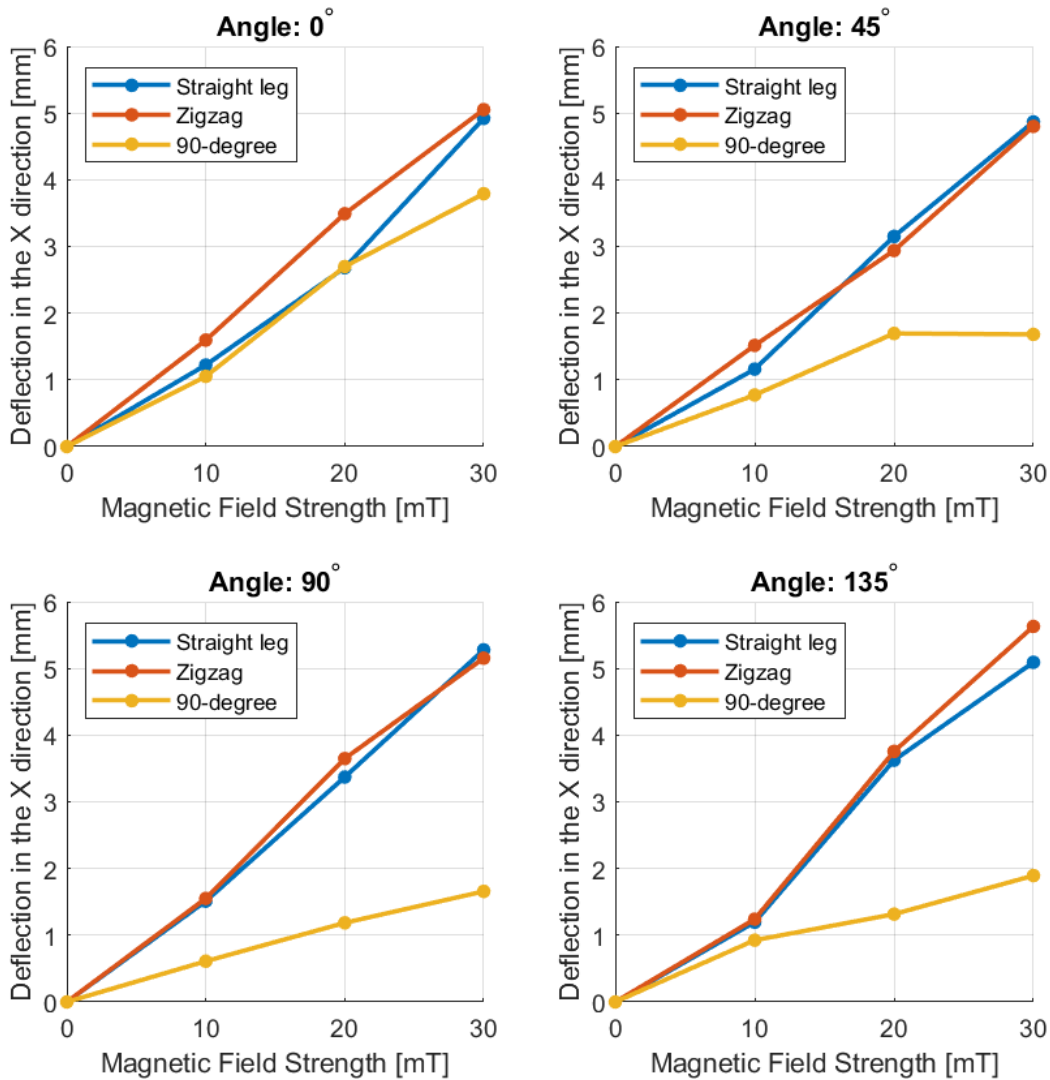


Figure 21: The results of the single-legged performance of the three legs: The maximum deflection of the leg in the X direction.

The results of the deflection in the X direction are shown in Fig. 21. From these results, it can be observed that the deflection for the Straight leg, Zigzag leg and 90-degree leg are closely matched in the 0-degree direction. However, the 90-degree magnetization patterned leg performs significantly worse in all directions of the rotating magnetic field. The results also show no significant increase or decrease in deflection in the X direction for movements over the diagonal (45° and 135°) for the Straight leg and Zigzag leg.

4.2.2 Deflection in the Y direction

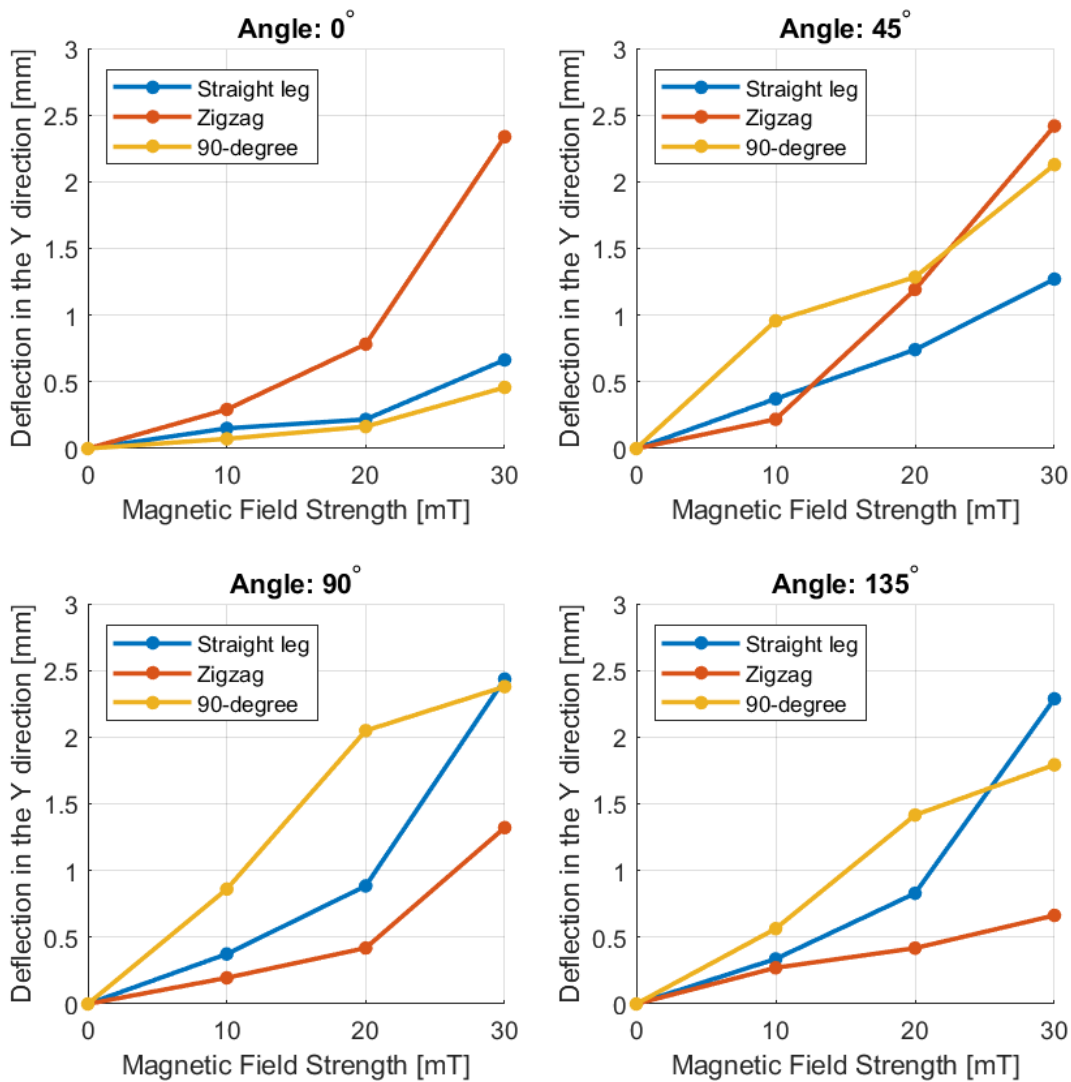


Figure 22: The results of the single-legged performance of the three legs: The maximum deflection of the leg in the Y direction.

Fig. 22 displays the deflection of the legs in the Y direction, indicating deflection in the non-compliant direction. From Fig 22, it can be seen that the Zigzag leg performs significantly worse in the angle 0° than the other two. For the other three angles, the 90-degree leg and Straight leg seem to perform similarly, with the Zigzag leg showing a lower deflection in the angles 90° and 135°.

4.2.3 Deflection in the Z direction

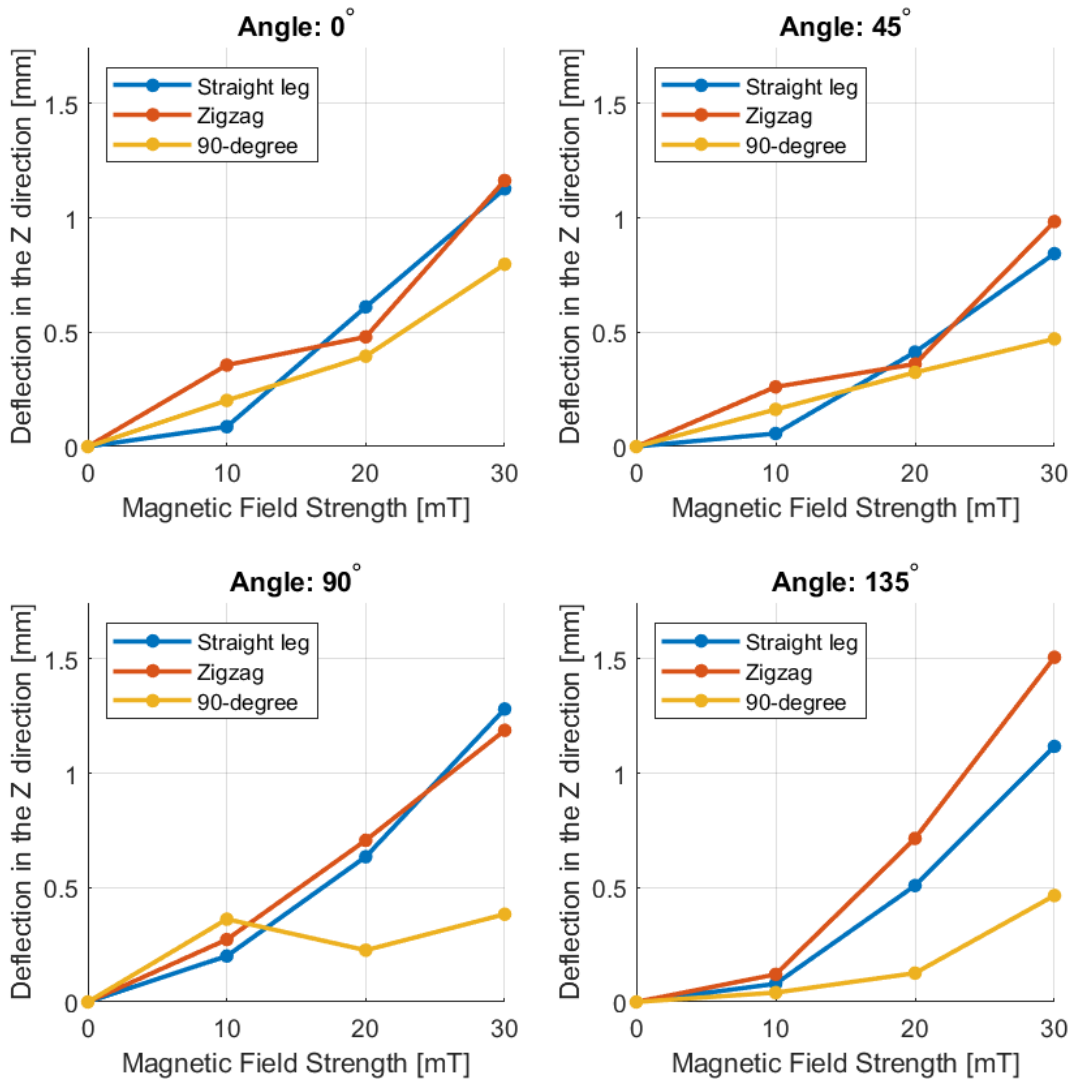


Figure 23: The results of the single-legged performance of the three legs: The maximum deflection of the leg in the Z direction.

In Fig. 23 the deflection of the legs in the Z direction can be observed. From this graph, one can observe that the performance of the Straight leg and Zigzag leg are similar to the results from the maximum deflection in the X direction with the 90-degree leg falling behind, particularly in the directions 90° and 135°.

4.3 Power-/Return stroke ratio

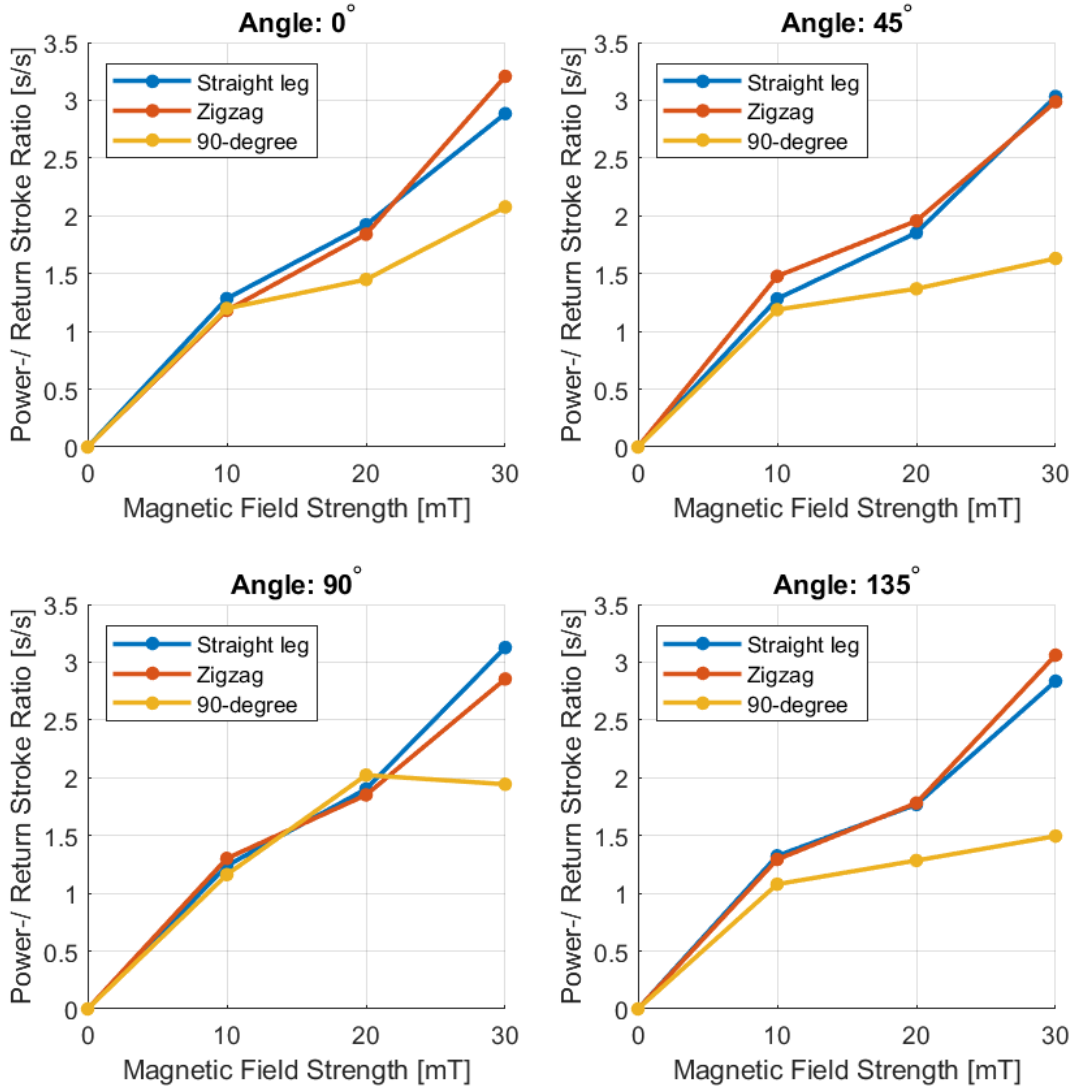


Figure 24: The results of the single-legged performance of the three legs: The Power-/ Return Stroke ratio T_p/T_r

The results of the Power-/Return stroke ratio T_p/T_r measurements for each direction are shown in Fig. 24. From these graphs, it can be observed that the Zigzag and Straight leg perform very similarly, with the 90-degree leg having a lower T_p/T_r as the magnetic field strength increases, especially at 135° angle.

4.4 Height Delta

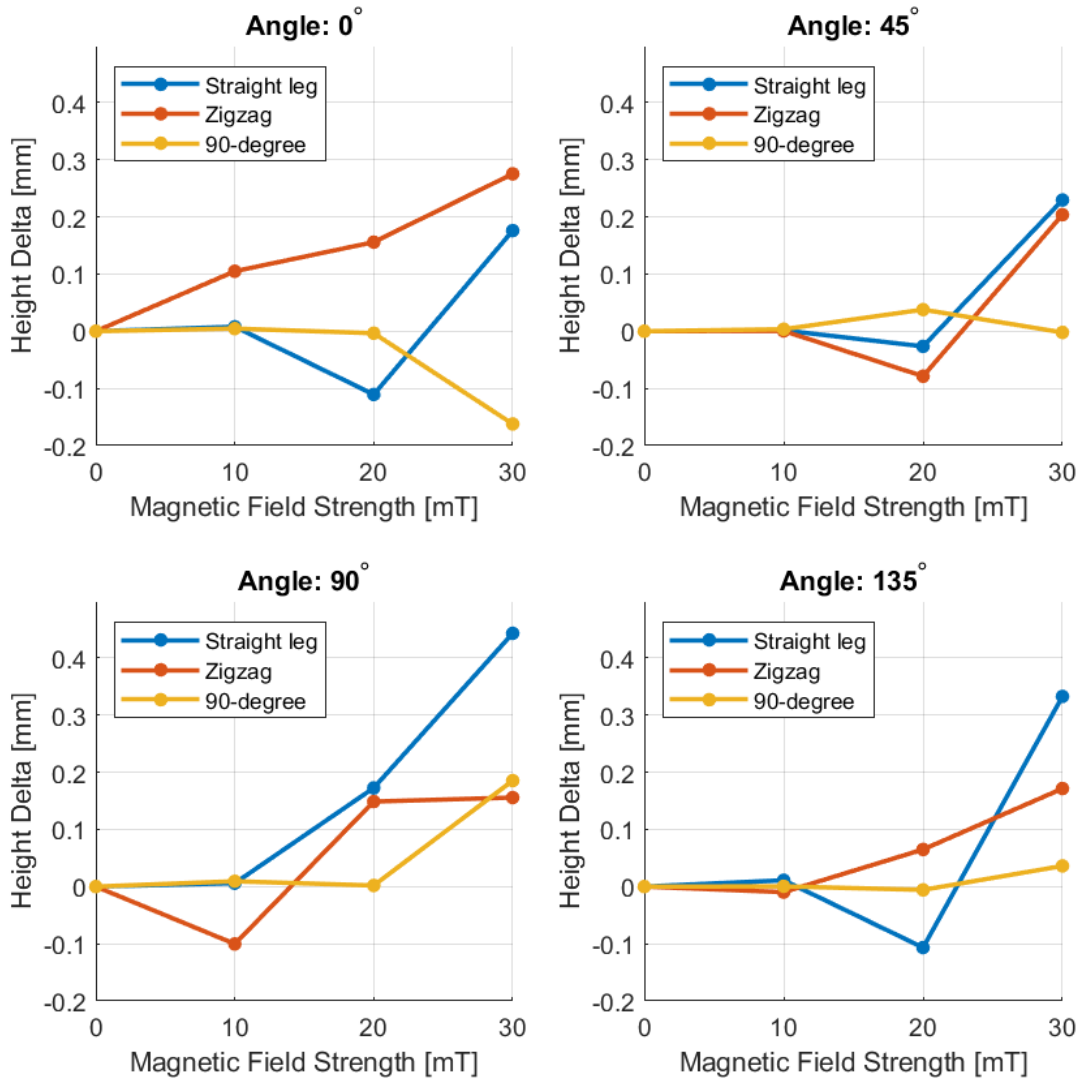


Figure 25: The results of the single-legged performance of the three legs: The height delta.

In Fig. 25 the results of the height delta are shown. From figure 25 it can be observed that the height delta for low magnitudes of the magnetic field B , the height delta tends to zero (or even negative). At higher magnitudes, the height delta seems to increase for the Zigzag leg and Straight leg, with the 90-degree leg remaining near zero.

5 Discussion

Based on the observations made in the results from the experiments and simulation several points and considerations need to be discussed.

1. **Similar results Zigzag leg and Straight leg:**

The results of the straight leg and Zigzag leg design show very similar results. The Zigzag design performs slightly worse in the maximum deflection in the Y direction which indicates the out-of-plane direction. This means that this type of leg will deviate from its path when moving in the compliant direction, which is suboptimal for achieving omnidirectional motion. The other performance indicators show very similar results, which brings a promising perspective for future research.

2. **Negative height delta for lower magnetic field strengths:**

Curiously the height delta becomes negative for the lower magnetic field strengths. This height delta is however of a very low magnitude (max -0.15mm) and is expected to be a measurement error.

3. **Performance issues 90-degree leg:**

The results of the 90-degree leg show that it performs significantly worse in all categories except the deflection in the Y-direction. By inspection of the video footage, this lower deflection is a direct result of the 90-degree leg having a torque rotating along the Z direction due to the magnetic dipole orientation. This is mainly present at the angles where the magnetic orientation of the dipoles also has a component in the Y-direction. Therefore the out-of-plane deflection is small, but a torque rotating around the Z-axis means that the leg will start to rotate around its axis which is unfavourable. This torque also influences the results of the T_p/T_r of the 90-degree polarised leg, making it less favourable.

4. **Challenging Zigzag design:**

The similar results of the Zigzag design could be influenced by the fact that the moulds for the magnetization pattern of the Zigzag leg were less accurate than wanted due to the difficulty of accurately making the desired magnetization patterns.

5. **Discrepancies due to measurement methods:**

Due to the measuring being done with cameras, which have a limited resolution compared to more accurate sensors (lasers). Therefore there could be discrepancies in the measurements which can cause an error in the measurement data.

6. **Limitation of Cosserat rod model simulation:**

The Cosserat rod simulation was not able to simulate the behaviour of a rotating magnetic field due to there not being a so-called 'history function' where the data for a cycle could be stored. Therefore, the simulation could only store the deflection of the rod in an ideal situation (there is a static angle imposed on the leg). Therefore the results of the simulations were only compared to the experiments in the X- and Z-direction for the angle 0° .

7. **Influence of gravity on simulation:**

In the Cosserat rod model simulation, the influence of gravity was found to be less than 5% of the total deflection, therefore for computational savings the gravity could be turned off for further research.

8. **Discrepancies between simulated and experimental 90-degree leg**

The results of the simulated and experimented 90-degree differ. This could be due to the simulated 90-degree leg being magnetized perfectly in one plane, while the experimental setup will perform worse already when it is shifted 1 degree out of the plane, which can happen easily due to manufacturing.

These points provide insight into the difficulty of analysing the performance characteristics of the MPC legs on omnidirectional locomotion efficiency. Addressing these factors will be essential in progressing the design and practical implementation of different magnetized leg patterns for omnidirectional soft robots.

6 Conclusion and Future research

The goal of this research was to investigate the performance indicators of different leg magnetization patterns, inspired by biomimetic gaits. From this foundation, three different leg magnetization patterns were studied. The Straight leg magnetization pattern served as the benchmark for this research, with the Zigzag and 90-degree patterned MPC legs as new designs. The maximum deflection of these legs was first studied in the Cosserat Model to find if they were suitable for omnidirectional motion, whereafter samples were made and tested in an experimental setting. The results of the experiments showed promising potential for the Zigzag leg as an alternative for the Straight leg with it performing on par on most performance indicators. The 90-degree leg performed significantly worse in all categories which was caused by the leg having a torque around the longitudinal direction (along the leg) when testing along different axes than the angle 0° .

For further research, research could expand into the behaviour of legs with a gradient of magnetic dipoles in the magnetic legs. This would mean that not only the angle but also the magnitude of the internal magnetization would change. Also, different cycle times can be researched to investigate the effect on the performance indicators.

References

- [1] V. K. Venkiteswaran, D. K. Tan, and S. Misra, “Tandem actuation of legged locomotion and grasping manipulation in soft robots using magnetic fields,” *Extreme Mechanics Letters*, vol. 41, p. 101023, 11 2020.
- [2] V. Experimente, “Magnetic field of two helmholtz coils.” Available online.
- [3] Q. Lu, K. Choi, J.-D. Nam, and H. J. Choi, “Magnetic polymer composite particles: Design and magnetorheology,” *Polymers*, vol. 13, p. 512, 2 2021.
- [4] ElectronicsTutorials, “Magnetism.” Available online.
- [5] V. K. Venkiteswaran, “Design flexible and soft robots.” Lecture slides, 2024. Lecture slides from the course “Design Flexible and Soft Robots” at University of Twente.
- [6] A. Doroudchi and S. Berman, “Configuration tracking for soft continuum robotic arms using inverse dynamic control of a cosserat rod model,” in *2021 IEEE 4th International Conference on Soft Robotics (RoboSoft)*, pp. 207–214, IEEE, 4 2021.
- [7] W. Pirker and R. Katzenschlager, “Gait disorders in adults and the elderly,” *Wiener klinische Wochenschrift*, vol. 129, pp. 81–95, 2 2017.
- [8] J. S. Van Der Veen, “Bsc thesis: Design of a magnetic soft robot capable of omni-directional motion,” 7 2023.
- [9] M. Runciman, A. Darzi, and G. P. Mylonas, “Soft robotics in minimally invasive surgery,” *Soft Robotics*, vol. 6, pp. 423–443, 8 2019.
- [10] C. Wang, V. R. Puranam, S. Misra, and V. K. Venkiteswaran, “A snake-inspired multi-segmented magnetic soft robot towards medical applications,” *IEEE Robotics and Automation Letters*, vol. 7, pp. 5795–5802, 4 2022.
- [11] X. Yang, R. Tan, H. Lu, and Y. Shen, “Starfish inspired milli soft robot with omnidirectional adaptive locomotion ability,” *IEEE Robotics and Automation Letters*, vol. 6, pp. 3325–3332, 4 2021.
- [12] D. ten Berge, “Design of magnetically actuated soft robots on mucous terrain,” August 2021. Examination Committee: Prof. Dr. S. Misra, Dr. V. Kalpathy Venkiteswaran, Dr. S.U. Yavuz.
- [13] “ECOFLEX_SERIES_TB.” Technical Bulletin.

A Appendix

During the preparation of this work, the author used ChatGPT in order to checking writing for spelling mistakes and debug MATLAB data analysis code. After using this tool/service, the author reviewed and edited the content as needed and takes full responsibility for the content of the work.

A.1 List of Parameters

Table A.1: Range of tested parameters for single-legged performance

Parameter	Description	Range	Unit
B	Magnetic field strength	[10, 20, 30]	mT
t	Magnetic field cycle time	4000	ms
θ	Magnetic field angle	[0, 45, 90, 135]	$^\circ$
-	Rotation orientation	Clockwise	-

Table A.2: Simulation parameters

Parameter	Description	Value	Unit
E	Young's modulus	125	kPa
I	Moment of inertia	1.33e-12	m^{-4}
L	Length of the beam	6	mm
W	Width of the beam	2	mm
ν	Poisson' ratio	0.48	
μ	Mean particle size	5	μm
μ_V	Magnetic moment per unit volume	60e5	Am^{-1}
dS	Spatial discretization	0.3	mm

Table A.3: Dimensions of the moulds

Indicator	Description	Value	Unit
a	Width cast	2	mm
b	Height cast	6	mm
c	Width cast	2	mm
d	Height cast	6	mm
e	Length Segment	2.3	mm
f	Angle	$\frac{\pi}{6}$	rad
g	Height cast	4	mm
h	Width cast	4	mm
i	Height Segment	2	mm

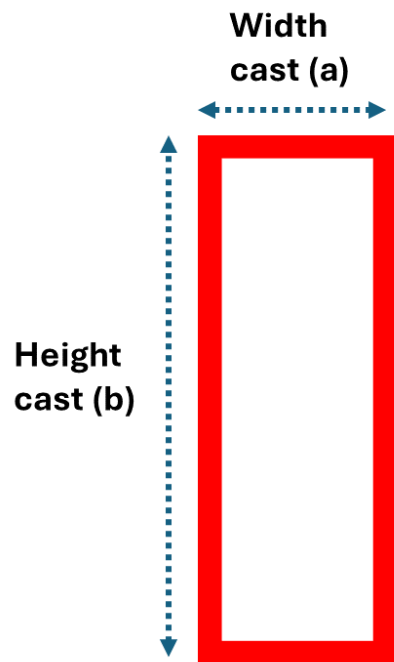


Figure A.1: Dimensions of the Straight MPC mould.

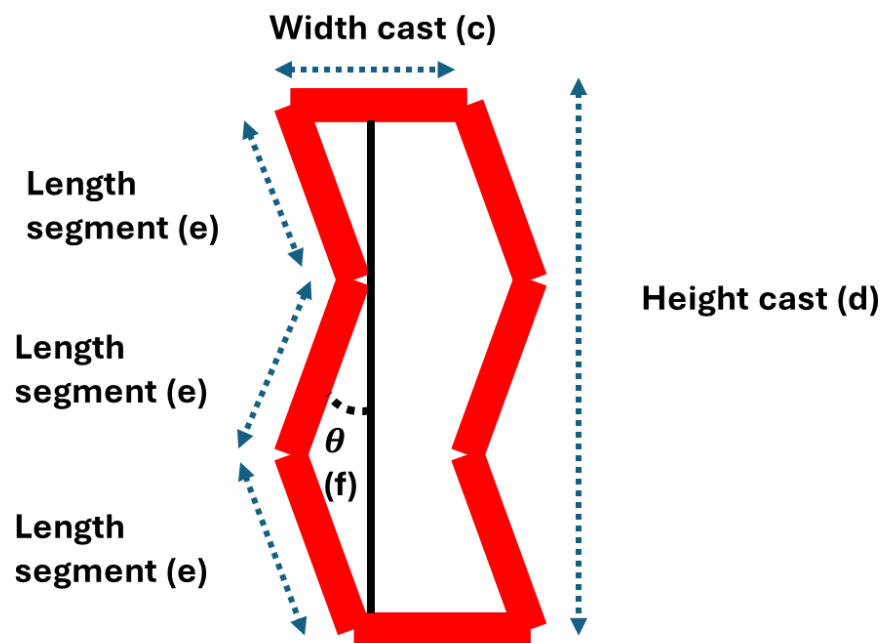


Figure A.2: Dimensions of the Zigzag MPC mould.

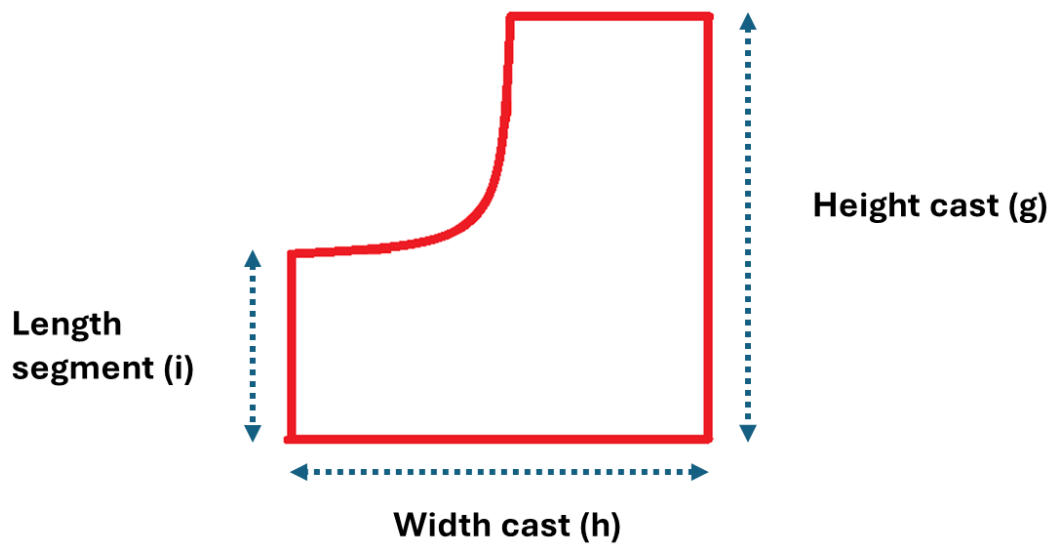


Figure A.3: Dimensions of the 90-degree MPC mould.